Arabian Journal of Geosciences (2018) 11: 440
https://doi.org/10.1007/s12517-018-3749-2

ICIEM 2016

Adsorption of nickel(II) and chromium(III) from aqueous phases on raw smectite: kinetic and thermodynamic studies

Sana Ghrab[1] · Samir Mefteh[2,3] · Mounir Medhioub[2] · Mourad Benzina[1]

Received: 27 October 2017 / Accepted: 19 July 2018 / Published online: 13 August 2018

Abstract

The ability of Tunisian smectite, collected from Aleg Formation (Jebel Romena), in the adsorption of nickel (Ni(II) and chromium (Cr(III)) cations from aqueous solutions has been studied through a bath adsorption mechanism with respect to different optimal parameters including the amount of adsorption, pH, and contact time. The characterization of a smectite sample was performed using XRD, XRF, FT-IR, SEM, BET-specific surface area techniques, thermo-gravimetric analyses, and CEC. The process of adsorption kinetics was examined using the pseudo-first-order, the pseudo-second-order, and the intraparticle diffusion models. The results revealed that the adsorption of Ni(II) and Cr(III) cations was according to the pseudo-second-order model. The changes of the thermodynamic parameters such us the Gibbs free energy (ΔG), the enthalpy (ΔH), and entropy (ΔS) attested, spontaneous and endothermic between 10 and 40 °C.

Keywords Smectite · Nickel · Chromium · Kinetic · Thermodynamic

Introduction

The discharge of the heavy metals into the environment is a critical pollution problem. Unlike organic pollutants, the heavy metals are not biodegradable. They keep accumulating in the organisms and to incorporate within the food chains through multiple pathways, which causes severe harm to human health (Lu et al. 2009; Amzal et al. 2009; Nagajyot et al. 2010; Ghnainia et al. 2016). Consequently, toxic heavy metals including zinc, nickel, copper, lead, chromium, cadmium, and mercury are of special concern in the treatment of industrial wastewater.

This article is part of the Topical Collection on *Water Resource Management for Sustainable Development*

✉ Sana Ghrab
sana.ghrab@yahoo.fr

[1] University of Sfax, BP W 3018, Sfax, Tunisia

[2] Faculty of Science, Department of Geology, University of Sfax, BP 3018, Sfax, Tunisia

[3] Laboratory of Valorization of Useful Material, CNRSM, BP 273, 8020 Soliman, Tunisia

The toxicity of chromium ions to the mammals and the aquatic organism is approved. For mammal, the toxicity manifests also by other heavy metal ions, such as Cr(III), generally, due to her lower solubility and her little mobility in the ecosystem compartments of heavy metals. The chromium ions are mentioned by the International Agency for Research on Cancer (IARC 2012) as strong carcinogenic agent, which changes the DNA transcription process (Nandy et al. 1990; Wielinga et al. 2001; Wang et al. 2012). At excessive concentrations, Nickel (Ni(II)) induces lungs, nose, and bone cancers. For example, the dermatitis is the major consequence of the exposure to nickel, likely costume jewelry and coins. Moreover, Ni carbonyl [Ni (CO)] has been considered as lethal to humans at atmospheric exposures of 30 ppm for 30 min (Beliles 1979; Natasha and Vernon 2006). The acute poisoning of nickel causes dizziness, headache, fast respiration, nausea and vomiting, dry cough and breath shortness, chest pain and tightness, cyanosis, and extreme weakness (ATSDR 2003).

Nowadays, many treatment technologies have been developed to remove the heavy metal ions from water and wastewater such us chemical precipitation (Villa-Gomez et al. 2011; Mbamba et al. 2015), ion exchange processes (Dabrowski et al. 2004; Kang et al. 2004; Figoli et al. 2010; Ahmad et al. 2011), coagulation (Kurniawan et al. 2006; Pang et al. 2011), and adsorption. Among the best techniques for the removal of heavy metals from wastewater is adsorption, because the adsorption is a reversible process and the adsorbent can be regenerated by simple desorption process for another use (Pan et al. 2009). Further, the adsorption mechanism is characterized by low maintenance cost, high capacity of elimination, and ease of operation.

In addition, the adsorption process has come to the forefront as one of the popular techniques for heavy metal removal from water/wastewater. Many studies developed a new adsorbent, such as activated phosphate rock (Elouar et al. 2008; Boujelben et al. 2008), activated carbon (Baccar et al. 2009; Omri et al. 2016), biomaterials (Wahaba et al. 2011; Ghrab et al. 2017a), and especially clay minerals (Chaari et al. 2008; Hamdi and Srasra 2012; Eloussaief and Benzina 2010; Ghrab et al. 2013; Eloussaief et al. 2014; Sdiri et al. 2016), characterized by a low-cost, large specific area, chemical and mechanical stability, layered structure, and high cation exchange capacity. These important characteristics could remove significantly the undesirable metals from wastewater.

In this study, a Tunisian smectite sample (R5) was characterized using X-ray diffraction (XRD), chemical analysis, Fourier transform infrared spectroscopy (FT-IR), thermal behavior, and scanning electron microscopy (SEM). Later, batch adsorption experiments were performed to evaluate the adsorption properties of the (R5) toward nickel(II) and chromium(III). In order to understand the adsorption mechanism, kinetic and thermodynamic model studies were also examined.

Materials and methods

Adsorbent

The smectite sample (R5) was collected from Aleg Formation in Jebel Romana. It is early Coniacian Age. Jebel Romana is located in the N-E termination of the anticline Zemlet El Bidha. (R5) was kept in an oven at 60 °C.

Characterization of smectite sample

The mineralogical analysis was determined out using a Philips® X-Pert diffractometer with Cu K_α radiation. The diffraction data results were analyzed with the X powder® computer program (Martín-Ramos 2004). For minerals quantification, the data results obtained by the classical method (area measurement of the peaks and relative power) were corrected according to the chemical composition of rock, following López-Galindo et al. (1996). The relative error was mentioned by 5%.

The chemical composition of the major elements of the total rock (R5) was obtained by XRF and flame-photometric methods, using a spectrometer of the type BRUKER S4 Pioneer X-ray Fluorescence, associated in the anode with X-ray RH (60 Kv, 150 my). Quantification was determined by the fundamental method of parameters using the software related to the equipment (Spectra Plus).

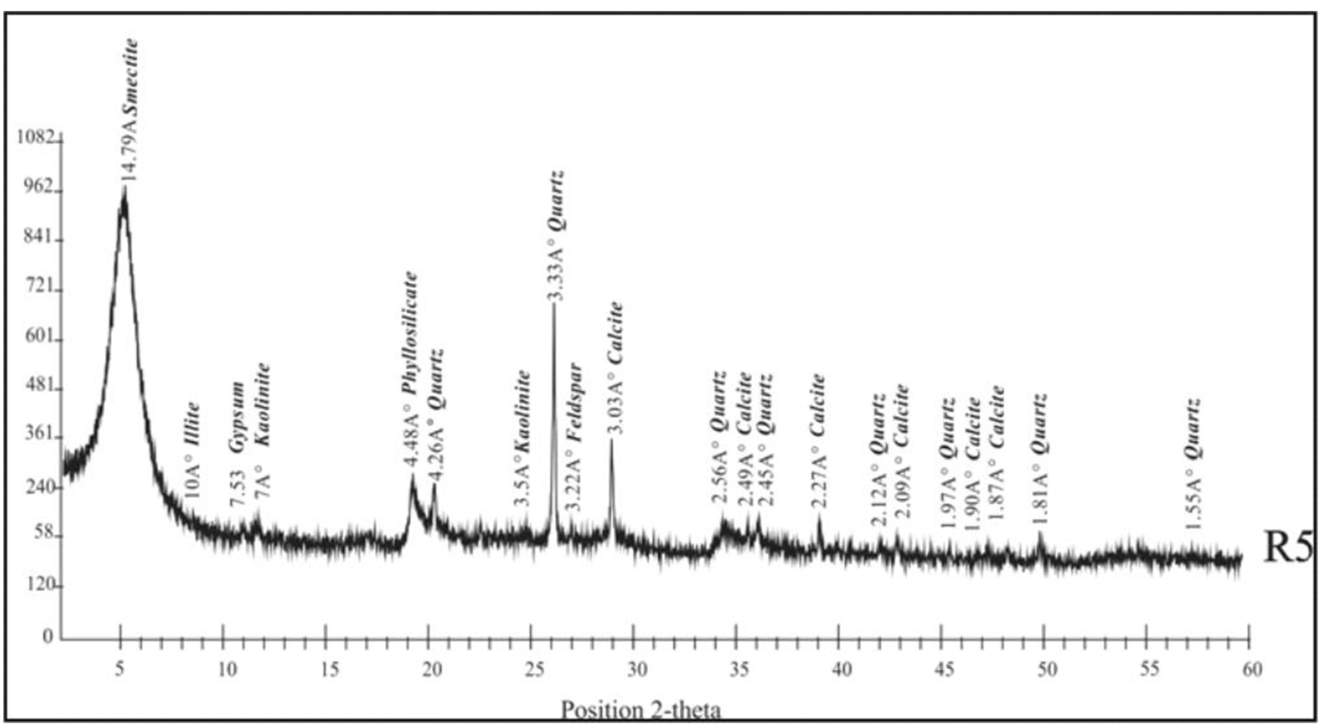

Fig. 1 Diffractogram XRD of total rock of adsorbent smectite clay R5

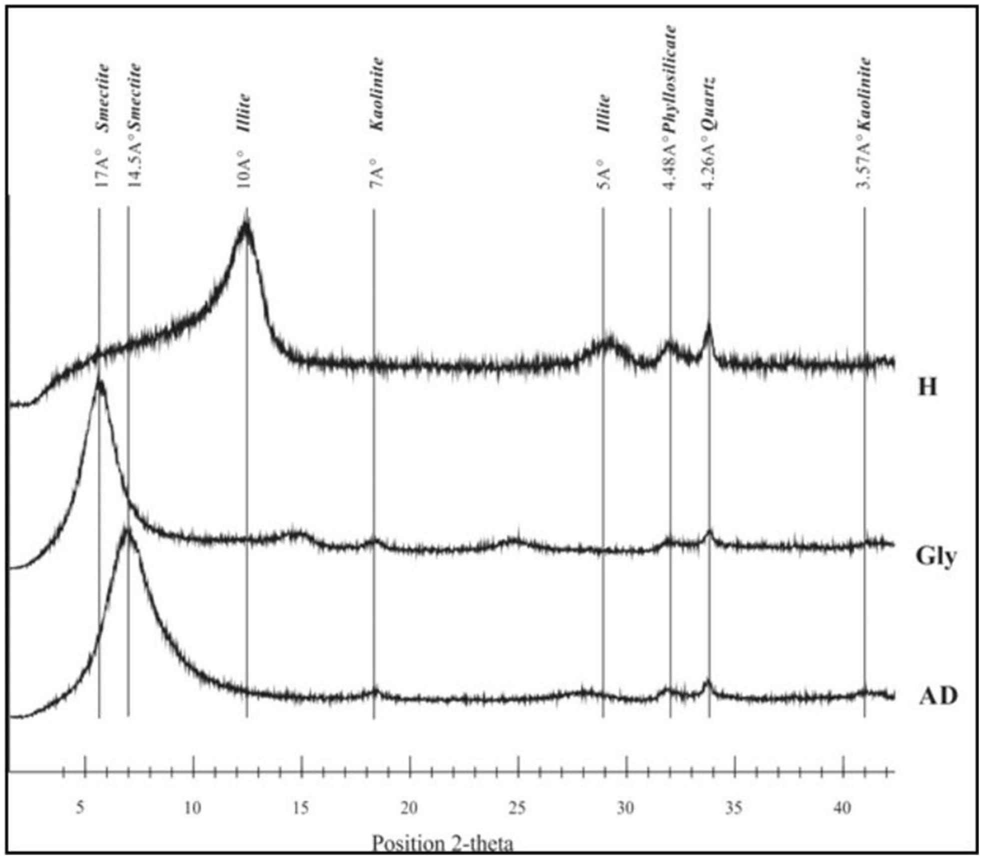

Fig. 2 Diffractogram XRD of oriented aggregates of adsorbent smectite clay R5

The FT-IR spectrum was obtained with a Nicole Impact 410 FT-IR spectrophotometer. The sample is depressed in KBr pellet between 400 and 4000 Cm^{-1}.

Thermogravimetric analyses were obtained using 1 g of sample, analyzed with TGA-50 SHIMADZU equipment operating in an air atmosphere, with a heating rate of 20 °C/min. TGA/DTA curves were obtained between 0 and 950 °C range.

A detailed study of the morphology and texture of the selected clay sample (R5) was carried out by the Scanning Electron Microscope AURIGA (FIB-FESEM) of Carl Zeiss SMT with high resolution (FESEM) and with the tension of variable acceleration.

The specific surface area was determined by Brunauer-Emmet-Teller (BET) method (Micromrtrics ASAP 2020 V3.04 H). The N_2 adsorption experiments were performed after a suitable thermal treatment (150 °C) under vacuum (10^{-4} Pa) for 24 h.

The cation exchange capacities (CEC) were estimated by washing thoroughly the sample with deionized water to eliminate superficial cations, and then, 1 g of (R5) powder was dispersed in 25 ml (1 M) aqueous solution of tetramethylammonium bromide to displace the constituent cations. The dispersion was shaken overnight at 50 rpm in water bath with 25 ± 1 °C. The content of the dispersion (Na^+, Ca^{2+}, and Mg^{2+}) in solution was determined by atomic absorption spectroscopy (PerkinElmer Spectrometer (5100 mod)), and the CEC was calculated as the sum of exchangeable cations, expressed in meq/100 g of (R5).

Adsorbate

All chemical reagents used were obtained from Fluka (purity 99%). A stock solution of each metal—Ni(II) (1041.09 ppm)

Table 1 Mineralogical composition of adsorbent smectite clay R5 (weight%/weight)

Sample	Total rock mineralogy						
R5	Clay minerals			Non clay minerals			
	Smectite	Illite	Kaolinite	Quartz	K-Feldspar	Calcite	Gypsum
	64	4	8	8	1	8	7

Table 2 Major element content of adsorbent smectite clay R5 (%)

	SiO_2	Al_2O_3	Fe_2O_3	MnO	MgO	CaO	Na_2O	K_2O	TiO_2	P_2O_5	LOI
R5	43.52	15.28	6.49	0.03	2.16	7.26	0.46	0.92	1.04	0.13	18.8

and Cr(III) (1026.82 ppm)—was prepared by dissolving $NiSO_4$ 7(H_2O) and $CrCl_3$ 6(H_2O) in distilled water.

Batch adsorption experiments

Batch adsorption was selected as an appropriate technique in the current study. The experiments were carried out by mixing of 0.5 g of (R5) sample with 50 ml of solutions containing heavy metals of the desired concentration. After equilibrium, suspensions were filtered and analyzed by the atomic absorption spectrophotometer (HITACHI model Z-6100).

To investigate the kinetic adsorption, a set of Erlenmeyer was prepared as described above, but then shaken for 2, 5, 10, 20, 30, 60, and 120 min. The initial concentration of 20 mg/L was the same in all of the kinetic study, as was the temperature (25 °C).

The thermodynamic studies of the metals adsorption were investigated by varying the concentration of each metals from 1 to 50 mg/L. The experiment isotherms were realized at 10 and 40 °C.

Results and discussion

Characterization of the smectitic clay adsorbent

The X-ray diffraction analysis of total rock (Fig. 1) and oriented aggregates (Fig. 2) indicates that the adsorbent clay R5 is mostly composed of phyllosilicates (76%) and associated minerals (24%). The mineralogical composition of phyllosilicates is fairly variable; it is composed of smectite (64%), with a weak percentage of kaolinite (8%) and illite (4%). Quartz (8%), calcite (8%), gypsum (7%), and potassium feldspar (1%) are associated minerals in this adsorbent smectitic clay (Table 1).

The adsorbent smectitic clay of Aleg Formation is characterized by a significant rate of Si (43.52%) and Al (15.28%) (Table 2). The enrichment of (R5) with aluminosilicate is confirmed by the significant rates of silica and aluminum. The (R5) sample is rich in iron oxide, CaO, and MgO, which verifies the high loss of ignition (LOI).

The FT-IR spectrum (Fig. 3) is correlated with the results obtained following the mineralogical characterization and chemical analysis. This confirms the presence of smectite (915 cm^{-1}) and quartz (780 cm^{-1}). Furthermore, these analyses prove that mineral surface clay is negatively charged with SiO^- (470, 530, and 1040 cm^{-1}) and AlO^- (3620 cm^{-1}) (Ghrab et al. 2017b).

Results of thermal study (Fig. 4) show multiple endothermic peaks: The first stage weight loss (11.05 and 0.7%) with two endothermic peaks, respectively, at 113.68 and 267.89 °C corresponds to the loosely bound water molecules (Baran et al. 2001). The second stage loss (3.79%) with an endothermic peak at 519.56 °C is due to the deshydroxylation of the octahedral sheet (Brigatti et al. 2005). The third stage loss (2.36%) with an endothermic

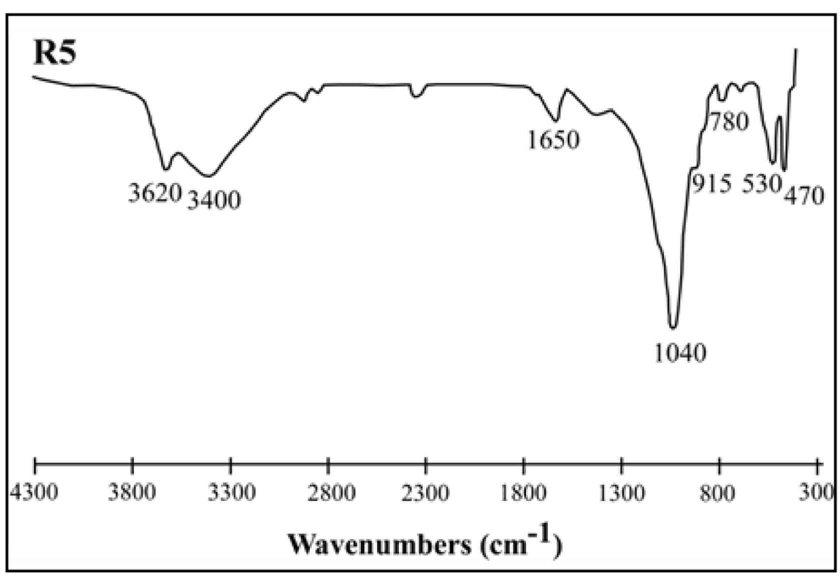

Fig. 3 FT-IR spectra of adsorbent smectite clay R5

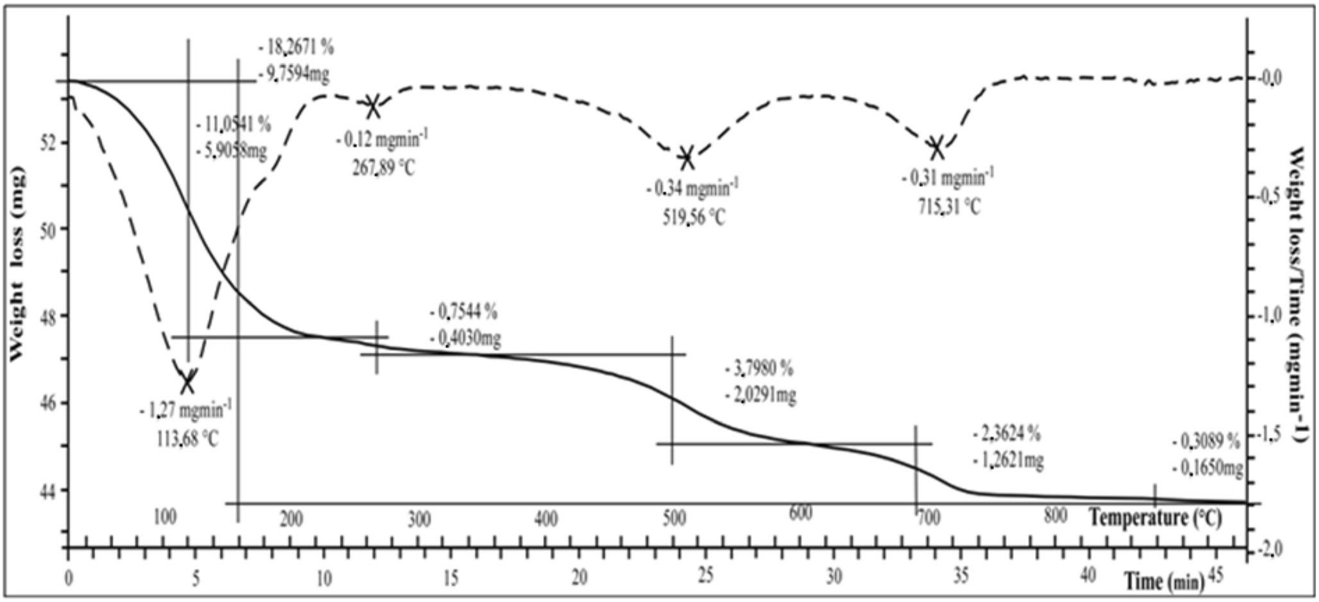

Fig. 4 TGA-DTA curves of R5 clay sample

peak at 715.31 °C is contributed to the decomposition of carbonates. Exothermic peak appeared at 989.56 °C due to the crystallization of new phases (Gillot 1987). The total weight loss is about 18.26%.

As for the identification of the morphology by SEM (Fig. 5), the sample R5 presents the layers of alumunosilicates with a honeycombs form having corrugated edges. This structure is characteristic of smectite clay (Azizi et al. 2013).

The BET method of N_2 adsorption-desorption was shown a BET surface area of R5 sample equal to 74.163 m^2/g. The result (Fig. 6) indicates that N_2 adsorption isotherm of R5 exhibits a sorption behavior of type II according to the classification of Brunauer, Deming, Deming and Teller (BDDT) (Tuccimei et al. 2015) with the appearance of hysteresis. The large uptake N_2 can be noticed close to the saturation pressure. This apparent step in adsorption branch following

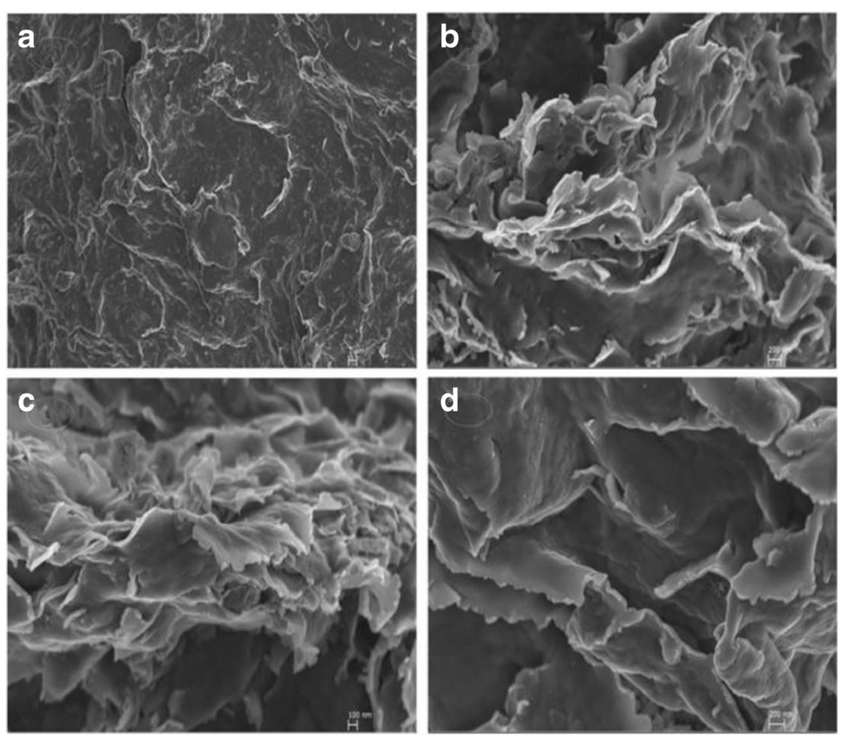

Fig. 5 SEM microphotographs of the adsorbent smectite clay R5 **a** (1 μm) **b** (200 μm) **c** (100 nm) **d** (200 nm)

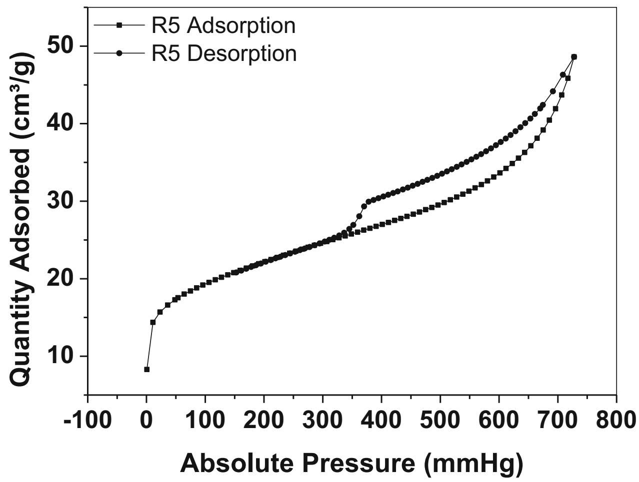

Fig. 6 N_2 adsorption/desorption isotherms of R5 sample of clay

by a sharp decline in the desorption branch confirms the presence of mesopore (Park et al. 2013).

CEC of the R5 sample are found to be 121.011 meq/100 mg. The total surface of the adsorbent smectitic clay is high which fosters the attachment of large amounts of metal ions. The main exchangeable cation is Ca^{2+} (95.437 meq/100 g), allowing this sample to be classified the calcium clay (Table 3).

Kinetics adsorption

Figure 7a presents the curve for Ni(II) and Cr(III) adsorption kinetics on (R5). The adsorption of heavy metal ions into R5 is found to occur rapidly in the first 10 min in the process, remaining virtually at equilibrium over time. At the beginning of adsorption, this rapidity is due to the active adsorption sites on the (R5) surface, which are more available to easily interact with metal ions. Afterwards, adsorption continues at a slower rate and finally reaches the equilibrium by the saturation of adsorption sites on (R5). The equilibrium is reached within 30 min for the both metal ions Ni(II) and Cr(III). However, having the highest affinity interaction, the adsorption system Cr/R5 is slower than the Ni/R5 one to reach the equilibrium state of the adsorption.

The adsorption kinetics was adjusted with the pseudo-first-order kinetic model (Ho 2004; Febrianto et al. 2009) (Fig. 7b), the pseudo-second-order kinetic model (Ho and McKay 1999; Ho et al. 2000) (Fig. 7c) and the intraparticle diffusion kinetic model (Karthika et al. 2010) (Fig. 7d) which are described in Table 4. The linear coefficients and the constants of kinetic models are given in Table 5.

The correlation coefficient for the pseudo second order kinetic model was higher than the other models ($R^2 = 1$, $R^2 = 0.999$) for Ni and Cr ions, respectively, attesting that the adsorption perfectly complies with the pseudo-second-order kinetic model and the adsorption process is controlled by the pseudo-second-order model. K_2 was employed to describe the chemisorption involving valency forces through the sharing or exchange of electrons between (R5) and heavy metal ions like covalent forces and ions exchanges (Ho 2006; Assameur and Boufatit 2012; Ghrab et al. 2018). According to Table 5, K_2 constant confirms that the adsorption rate of Ni(II) onto (R5) is more rapid than the adsorption of Cr(III) onto (R5). In addition, the theoretical q_e values determined from the pseudo-second-order kinetic model are in agreement with the experimental q_e values.

Moreover, intraparticle diffusion model was less suitable for the experimental values if compared with the second-order kinetic model. The curve does not pass through the origin (Fig. 7). This marked that the pseudo-second-order kinetics adsorption mechanism is not limited by intraparticle diffusion of the metal ions within (R5).

Thermodynamic study

The thermodynamic parameters ΔG, ΔH, and ΔG are presented in Table 6 and were determined using the following equations (Eqs. 6 and 7) and calculated values obtained slope and intercept Van't Hoff (Eq. 8) (Fig. 8).

The spontaneity of reactions is mentioned by the negative Gibbs free energy with a significant contribution of the positive entropy. These results confirmed the interaction of metal ions (Ni or Cr) with the reactive sites on the surface R5. The complexation of the heavy metal ions on the (R5) surface promotes the adsorption of new free ions. Consequently, heavy metal ions lead to an entropy increase.

The decrease in the Gibbs free energy with the increase of the temperature, identically for Ni and Cr, presents that the adsorption mechanism is favorable at higher temperature. In addition, the values of enthalpy of adsorption onto (R5) are positive; it indicates that the adsorption mechanism of Ni(II) and Cr(III) is an endothermic process, controlled by physical and chemical mechanisms of adsorption (Malkoc and Nuhoglu 2005; Huang et al. 2007).

Table 3 Exchangeable cation of the studied sample (meq/100 g)

Sample	Ca^{2+} (meq/100 g)	Mg^{2+} (meq/100 g)	Na^{+} (meq/100 g)	K^{+} (meq/100 g)	CEC (meq/100 g)
R5	95.43	15.09	9.11	1.36	121.01

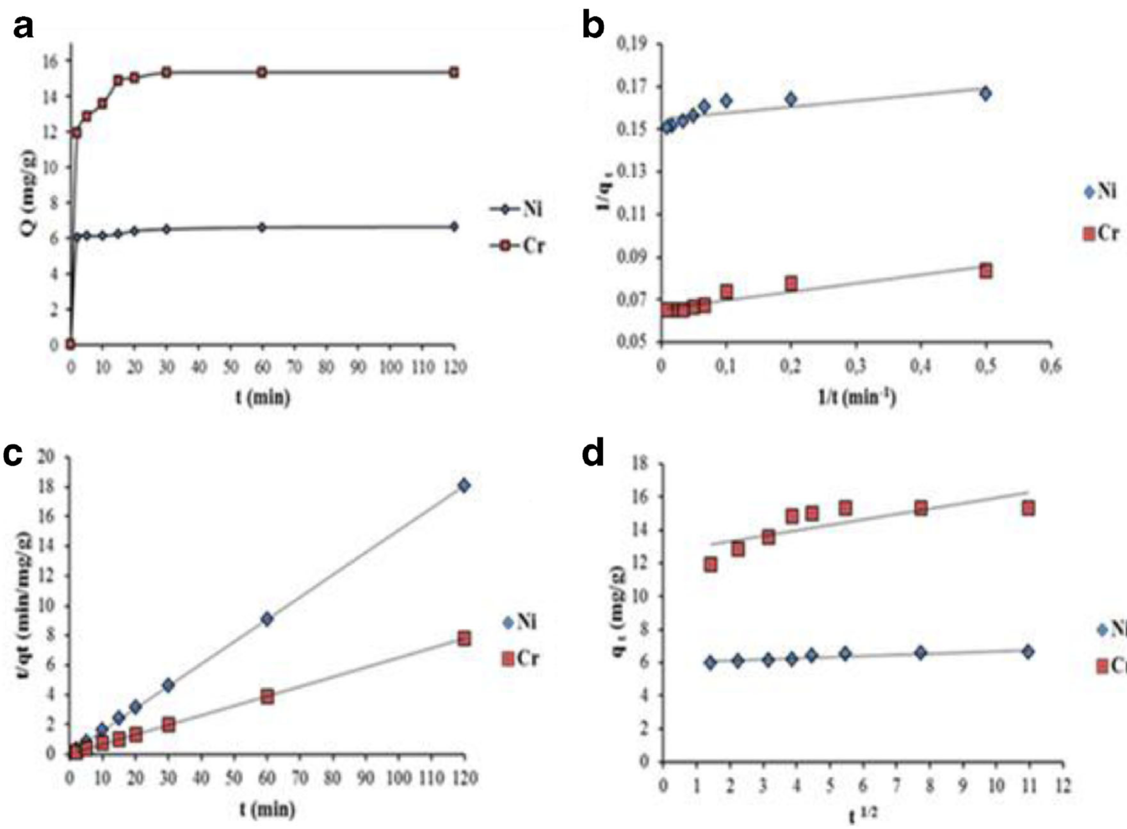

Fig. 7 Kinetic curve for nickel and chromium adsorption onto R5. **a** Adsorbed amount at equilibrium. **b** Pseudo-first-order kinetic model. **c** Pseudo-second-order kinetic model. **d** Intraparticle kinetic model

The positive values of entropy changes for Ni(II) and Cr(III) present that randomness increased at solid-liquid interface during the adsorption mechanism. Therefore, it could be inferred that the adsorption was propelled by entropy (Sheng et al. 2013).

Conclusion

The raw clay, originally from the Jebel Romana, Tunisia, was investigated for the removal of Ni(II) and Cr(III) from aqueous solution in the present study. The (R5) was characterized by XRD, FTIR, TGA–DTA, and SEM that were identified as smectite with a high BET surface area (74.163 m^2/g) and CEC (121.011 meq/100 mg). Furthermore, the ability of (R5) to remove Ni(II) and Cr(III) was evaluated using equilibrium and thermodynamics models.

The pseudo-second-order kinetic model shows the best correlation with the experimental kinetic data. The experimental q_e and the calculated (by the second-order model) q_e showed greater agreement for both heavy metal ions (q_e(Ni) = 6.660, q_e(Cr) = 15.479).

Table 4 Kinetic adsorption models used in this work and their parameters

	Equation	Linearized form	Parameters
Pseudo-first-order	$\frac{dq_t}{dt} = K_1(q_e - q_t)$ (Eq. 1)	$\frac{1}{q_t} = \frac{K_1}{q_e t} + \frac{1}{q_e}$ (Eq. 2)	q_e (mg/g): the adsorption capacity at equilibrium time q_t (mg/g): the adsorption capacity at time t t (min): contact time K_1: the rate constant of pseudo-first order kinetic model
Pseudo-second-order	$\frac{dq_t}{dt} = K_2(q_e - q_t)^2$ (Eq. 3)	$\frac{t}{q_t} = \frac{1}{(K_2 q_e ex2)} + \left(\frac{1}{q_e}\right)t$ (Eq. 4)	q_t (mg/g): the adsorption capacity at time t K_2: the rate constant of the pseudo-second-order kinetic model
Intraparticle diffusion	$q_t = K_d t^{1/2} + C$ (Eq. 5)	$q_t = K_d t^{1/2} + C$	q_t (mg/g): the adsorption capacity at time t K_d: the intraparticle diffusion rate constant C: the intercept

Table 5 Ni and Cr adsorption rate coefficients for pseudo-first-order model, pseudo-second-order model, and intraparticle diffusion model onto R5

	Pseudo first order (Eq. 2)	Pseudo second order (Eq. 4)	Intraparticle diffusion (Eq. 5)
Ni	$K_1 = 0.18$	$K_2 = 0.21$	$K_d = 0.07$
	$q_{eq} = 6.45$	$q_{eq} = 6.66$	$C = 0.97$
	$R^2 = 0.60$	$R^2 = 1$	$R^2 = 0.84$
Cr	$K_1 = 0.61$	$K_2 = 15.47$	$C = 12.67$
	$q_{eq} = 15.22$	$q_{eq} = 15.47$	$C = 12{,}677$
	$R^2 = 0.87$	$R^2 = 0.99$	$R^2 = 0.59$

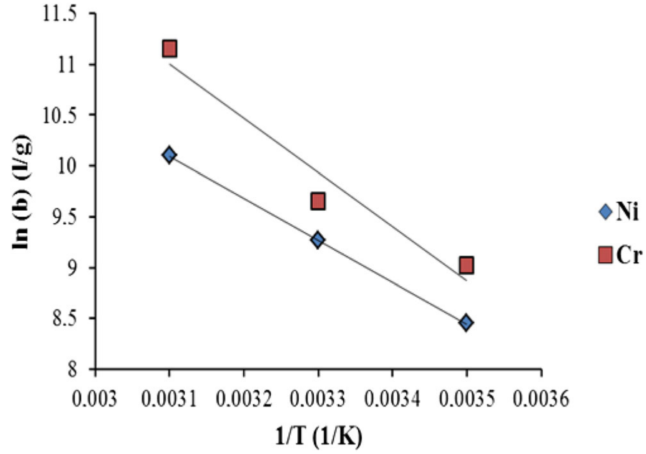

Fig. 8 Graphical representation of the Van't Hoff equation

The adsorption results were confirmed through stable complexes established between cations and reactive groups disposed on the raw clay surface. The complex behavior was determined based on the thermodynamic constants obtained by Van't Hoff correlation in the solid/liquid interface to give favorable results, and thermodynamic values showed that the process adsorption of Ni and Cr by R5 has endothermic enthalpy, negative Gibbs free energy, and positive entropy values. These thermodynamic values suggest the investigation of this worldwide available material to improve the heavy metals adsorption.

Currently, a large variety of adsorbent materials are used for heavy metal ion removal; the ideal adsorbent mandatorily should have interesting characteristics for industrial and environmental application. In this context, it is possible to conclude that the employed smectite (R5) is more economical than the commercially available adsorbents. Moreover, this raw clay is actually available and easily accessible in many geological outcrops in Tunisia, particularly in the Aleg Formation at Jebel Romana. Temperature, thermodynamic parameters, effect of concentration variation, and contact time are very important parameters that influenced the adsorption capacity in the real application of the adsorption process by these materials.

Table 6 Thermodynamic parameters for Cr and Ni adsorption onto R5

	T (K)	ΔG (J/mol) $\Delta G = -RTlnb$ (Eq. 6)	ΔH (kJ/mol) $\Delta G = \Delta H - T\Delta S$ (Eq. 7)	ΔS (J/(K mol)) $\ln b = \frac{\Delta S}{R} - \frac{\Delta H}{RT}$ (Eq. 8)
Ni	283	− 19.89	45.78	0.23
	298	− 22.94		
	313	− 26.43		
Cr	283	− 21.23	59.59	0.28
	298	− 23.92		
	313	− 29.08		

b equilibrium constant obtained from the Langmuir isotherm equation, *T(K)* temperature, *R* universal gas constant (8.314×10^{-3} kJ/kmol)

References

Ahmad AL, Majid MA, Ooi BS (2011) Functionalized PSf/SiO_2 nanocomposite membrane for oil-in-water emulsion separation. Desalination 268(1–3):266–269

Amzal B, Julin B, Vahter M, Wolk A, Johanson G, Akesson A (2009) Population toxico kinetic modeling of cadmium for health risk assessment. Environ Health Perspect 117:1293–1301

Assameur H, Boufatit M (2012) Contribution to the removal study of Co^{2+} ions by acid-activated clay from Maghnia (Algeria): equilibrium and kinetic studies. Desalin Water Treat 45(1–3):315–323

ATSDR (2003) Toxicological profile for pyrethrins and pyrethroids. Agency for Toxic Substances and Disease Registry, Atlanta

Azizi FM, Dib S, Boufatit M (2013) Removal of heavy metals from aqueous solutions by Algerian bentonite. Desalin Water Treat 51(22–24):4447–4458

Baccar R, Bouzid J, Feki M, Montiel A (2009) Preparation of activated carbon from Tunisian olive-waste cakes and its application for adsorption of heavy metals ions. J Hazard Mater 162:1522–1529

Baran B, Ertuk T, Sarikaya Y, Alemdaroglu T (2001) Workability test method for metals applied to examine a workability measure (plastic limit) for clays. Appl Clay Sci 20:53–63

Beliles RP (1979) The lesser metals. In: Oehme FW (ed) Toxicity of heavy metals in the environment, part 2. Marcel Dekker, New York, p 383

Boujelben N, Bouzid J, Elouar Z, Feki M, Jamoussi F, Montiel A (2008) Phosphorous removal from aqueous solution using iron coated natural and engineer adsorbents. J Hazard Mater 151:103–110

Brigatti MF, Laurora A, Malferrari D, Medici L, Poppi L (2005) Adsorption of $[Al(urea)_6]^{3+}$ and $[Cr\ (urea)_6]^{3+}$ complexes in the vermiculite interlayer. Appl Clay Sci 30:21–32

Chaari I, Fakhfakh E, Chakroun S, Bouzid J, Boujelben N, Feki M, Rocha F, Jamoussi F (2008) Lead removal from aqueous solutions by a Tunisian smectite clay. J Hazard Mater 156:545–551

Dabrowski A, Hubicki Z, Podkościelny P, Robens E (2004) Selective removal of the heavy metal ions from waters and industrial wastewater by ions exchange method. Chemosphere 56(2):91–106

Elouar Z, Bouzid J, Boujelben N, Feki M, Montiel A (2008) Heavy metal removal from aqueous solutions by activated phosphate rock. J Hazard Mater 156:412–420

Eloussaief M, Benzina M (2010) Efficiency of natural and acid-activated clays in the removal of Pb (II) from aqueous solutions. J Hazard Mater 178(1–3):753–757

Eloussaief M, Bouaziz S, Kallel N, Benzina M (2014) Valorization of El Haria clay in the removal of arsenic from aqueous solution. Desalin Water Treat 52(10–12):2220–2224

Febrianto J, Kosasih AN, Sunarso J, Ju YH, Indraswati N, Ismadji S (2009) Equilibrium and kinetic studies in adsorption of heavy metals using biosorbent: a summary of recent studies. J Hazard Mater 162: 616–645

Figoli A, Cassano A, Criscuoli A, Mozumder MSI, Uddin MT, Islam MA, Drioli E (2010) Influence of operating parameters on the arsenic removal by nanofiltration. Water Res 44:97–104

Ghnainia L, Eloussaief M, Zouari K, Abbes C (2016) Waste water treatment in petroleum activities: example of "SEWAGE" unit in the BG Tunisia Hannibal plant. Appl Petrochem Res 6(2):155–162

Ghrab S, Boujelben N, Medhioub M, Jamoussi F (2013) Chromium and nickel removal from industrial wastewater using Tunisian clay. Desalin Water Treat 52:2253–2260

Ghrab S, Benzina M, Lambert S (2017a) Copper adsorption from wastewater using bone charcoal. Adv Mater Phys Chem 7:139–147

Ghrab S, Eloussaief M, Lambert S, Benzina M, Bouaziz S (2017b) Adsorption of terpenic compounds onto organo-palygoskite. Environmental Sciences and Pollution Research. Online

Ghrab S, Balme S, Cretin M, Bouaziz S, Benzina M (2018) Adsorption of trepenes from Eucalyptus globulus onto modified beidellite. Appl Clay Sci 156:169–177

Gillot JE (1987) Clay in engineering geology. Elsevier Science Publishers, Amsterdam

Hamdi N, Srasra E (2012) Removal of phosphate ions from aqueous solution using Tunisian clays minerals and synthetic zeolite. J Environ Sci 24(4):617–623

Ho Y S (2004) Citation review of Lagergen kinetic rate equation on adsorption reactions. Akadémiai Kiado, Budapest, and Kluwer academic publishers, Dordrecht. Scientometrics 59, N° 1:171–177

Ho Y (2006) Review of second-order models for adsorption systems. J Hazard Mater 136(3):681–689

Ho YS, McKay G (1999) Pseudo second order model for sorption process. Process Biochem 34:451–465

Ho YS, McKay G, Wase DAJ, Foster CF (2000) Study of the sorption of divalent metal ions on the peat. Adsorpt Sci Technol 8:639–650

Huang YH, Hsueh CL, Huang CP, Su LC, Chen CY (2007) Adsorption thermodynamic and kinetic studies of Pb (II) removal from water onto a versatile AL_2O^{3-} supported iron oxide. Sep Purif Technol 55: 23–29

International Agency for Research on Cancer (IARC) (2012) Chromium, nickel and welding, IARC monographs on the education of carcinogenic risks to humans, 49. World Health Organization, Lyon

Kang SY, Lee JU, Moon SH, Kim KW (2004) Competitive adsorption characteristics of Co^{2+}, Ni^{2+} and Cr^{3+} by IRN-77 cations exchange resin in synthesized wastewater. Chemosphere 56:141–147

Karthika C, Vennilamani N, Pattabhi S, Sekar M (2010) Utilization of sago waste as an adsorbent for the removal of Pb (II) from aqueous solutions: kinetic and isotherm studies. Int J Eng Sci Technol 2(6): 1867–1879

Kurniawan TA, Chan GYS, Lo WH, Babel S (2006) Physico-chemical treatment techniques for wastewater laden with laden heavy metals. Chem Eng J 118:83–98

López-Galindo A, Torres-Ruiz J, González-López JM (1996) Mineral quantification in sepiolite–palygorskite deposists using X-ray diffraction and chemical data. Clay Miner 31:224–227

Lu XW, Wang LJ, Lei K, Huang J, Zhai YX (2009) Contamination assessment of copper, lead, zinc manganese and nickel in street dust of Baoji, NW China. J Hazard Mater 161:1058–1062

Malkoc E, Nuhoglu Y (2005) Investigation of nickel (II) removal from aqueous solutions using tea factory waste. J Hazard Mater B 127: 120–128

Martín-Ramos J D (2004) X-powder, a software package for powder X-ray diffraction analysis. Legal deposit G.R.1001/04. http://www.xpowder.com

Mbamba CK, Batstone DJ, Flores-Alsina X, Tait S (2015) A generalized chemical precipitation modeling approach in wastewater treatment applied to calcite. Water Res 68:342–353

Nandy T, Kaul SN, Pathe PP, Malika B (1990) Chromium recovery from spent chrome tan liquor. CEW XXV 20:90

Natasha AG, Vernon RM (2006) Assessment of public health risks associated with atmospheric exposure to PM2.5 in Washington, DC, USA. Int J Environ Res Public Health 3(1):86–97

Omri A, Wali A, Benzina M (2016) Adsorption of bentazon on activated carbon prepared from Lawsonia *inermis* wood: equilibrium, kinetic and thermodynamic studies. Arab J Chem 9(2):1729–1739

Pan BJ, Pan BC, Zhang WM, Lv L, Zhang QX, Zheng SR (2009) Development of polymeric and polymer-based hybrid adsorbents for pollutants from waters. Chem Eng J 151:19–29

Pang FM, Kumar P, Teng TT, Mohd OAK, Wasewar KL (2011) Removal of lead, zinc and iron by coagulation–flocculation. J Taiwan Inst Chem Eng 42:809–815

Park Y, Ayoko GA, Kurdi R, Horváth E, Kristóf J, Frost RL (2013) Adsorption of phenolic compounds by organoclays: implications for the removal of organic pollutants from aqueous media. J Colloid Interface Sci 15(406):196–208

Sdiri A, Khairy M, Bouaziz S, El-Safty S (2016) A natural clayey adsorbent for selective removal of lead from aqueous solutions. Appl Clay Sci 126:89–97

Sheng GP, Xu J, Luo HW, Li WW, Li WH, Xie Z, Wei SQ, Hu FC, Yu HQ (2013) Thermodynamic analysis on the binding of heavy metals onto extracellular polymeric substances (EPS) of activated sludge. Water Res 47:607–614

Tuccimei P, Mollo S, Soligo M, Scarlato P, Castelluccio M (2015) Real-time setup to measure radon emission during rock deformation: implications for geochemical surveillance. Geosci Instrum Methods Data Syst 5:39–62

Villa-Gomez D, Ababneh H, Papirio S, Rousseau DPL, Lens PNL (2011) Effect of sulfide concentration on the metal precipitates in inversed fluidized bed reactors. J Hazard Mater 192(1–15):200–207

Wahaba MA, Ben Hassineb R, Jellalia S (2011) Removal of phosphorus from aqueous solutions by Posidonia oceanica fibers using continuous stirring tank reactor. J Hazard Mater 189:577–585

Wang X, Mandal AK, Saito H, Pulliam JF, Lee EY, Ke ZJ, Lu J, Ding S, Li L, Shelton BJ, Tucker T, Evers BM, Zhang Z, Shi X (2012) Arsenic and chromium in drinking water promote tumorigenesis in a mousecolitis-associated colorectal cancer model and the potential mechanism is ROS-mediated Wnt/β-catenin signaling pathway. Toxicol Appl Pharmacol 262:11–21

Wielinga B, Mizuba M, Hansel CM (2001) Iron promoted reduction of chromate by dissimilatory iron-deducing bacteria. Environ Sci Technol 35:522–527